Journal of Sound and Vibration (2001) **247**(1), 59–76
doi:10.1006/jsvi.2001.3630, available online at http://www.idealibrary.com on IDEAL®

MOVING FORCE IDENTIFICATION STUDIES, I: THEORY

T. H. T. Chan, L. Yu and S. S. Law

Department of Civil & Structural Engineering, The Hong Kong Polytechnic University, Hung Hom, Kowloon, Hong Kong, E-mail: cetommy@polyu.edu.hk

AND

T. H. Yung

T.Y. Lin (Hong Kong) Consulting Engineers Limited, Suite D, 156, *Austin Road, Kowloon, Hong Kong*

(*Received* 27 *July* 2000, *and in final form* 17 *January* 2001)

Traditional ways to acquire information on truck axle and gross weight are expensive and subject to bias, and this led to the development of weight-in-motion (WIM) techniques. Most of the existing WIM systems have been developed to measure only the static axle loads. However, dynamic axle loads are also important. Some systems use instrumented vehicles to measure dynamic axle loads, but are subject to bias. All of this prompted the need to develop a system to measure the dynamic axle loads using an unbiased random sample of vehicles. This paper aims to introduce four methods in determining such dynamic axle loads from bridge responses. The four methods are interpretive method I, interpretive method II, time domain method, and frequency–time domain method. Examples and experiments in laboratory show that all the four methods are feasible and the time domain method and frequency–time domain method give very good results even when 5% noise is added to the simulated input data.

1. INTRODUCTION

Truck axle and gross weight information have applications in areas such as the structural and maintenance requirements of bridges and pavements. However, the traditional ways of acquiring this information are expensive and subject to bias, and this has led to the development of weigh-in-motion (WIM) techniques. Some of these techniques use road-surface systems, which make use of piezo-electric (pressure electricity), or capacitive properties to develop plastic mat or capacitive sensors to measure axle weight [1]. Under-structure WIM systems are also used in which sensors are installed under a bridge or a culvert and the axle loads are computed from the measured responses, e.g., AXWAY [2] and CULWAY [3]. These systems can only give the equivalent static axle loads. However, dynamic axle loads are also important as dynamic effects may increase static loads road surface damage by a factor between 2 and 4 [4]. Some systems use instrumented vehicles to measure dynamic axle loads [5], but are subject to bias. It is clear that there is a need to develop a system, which measures dynamic axle loads based on unbiased random sampling of vehicles. Four methods have been developed and presented in this paper for the determination of such dynamic forces from bridge responses which include measured bending moments, accelerations, and bending moments and accelerations.

0022-460X/01/410059 + 18 $35.00/0

2. EQUATIONS OF MOTION FOR MOVING LOADS

The moving force identification methods (MFIM) described in this paper are the inverse of the predictive analysis problems defined by O'Connor and Chan [6], which is based on simulating the structural response caused by a set of time-varying forces running across a bridge. Two models can be used for this kind of analysis; a 'beam-element' model and a 'continuous beam' model described below.

2.1. BEAM-ELEMENT MODEL

O'Connor and Chan [6] model the bridge as an assembly of lumped masses interconnected by massless elastic beam elements a shown in Figure 1, and the nodal responses for displacements and bending moments at any instant are given by equations (1) and (2) respectively.

$$\{Y\} = [Y_A]\{P\} - [Y_I][\Delta m]\{\ddot{Y}] - [\mathrm{Y_I}][\mathrm{C}][\dot{\mathrm{Y}}], \tag{1}$$

$$\{M\} = [M_A]\{P\} - [M_I][\Delta m]\{\ddot{Y}] - [\mathrm{M_I}][\mathrm{C}][\dot{\mathrm{Y}}], \tag{2}$$

where $\{P\}$ is the vector of wheel loads; $[\Delta m]$ is the diagonal matrix containing values of lumped mass; $[C]$ is the damping matrix; $\{M\}$, Y, $\dot{Y}$, $\ddot{Y}$ are the nodal bending moments, displacements, velocities, and accelerations respectively; $[Y_A]$, $[Y_I]$ are matrices for nodal forces to obtain nodal displacements, and $[M_A]$, $[M_I]$ are matrices for nodal forces to obtain nodal bending moments.

2.2. CONTINUOUS BEAM MODEL

Assuming the beam is of constant cross-section with constant mass per unit length, having linear, viscous proportional damping and with small deflections, neglecting the effects of shear deformation and rotary inertia (Bernoulli–Euler's beam), and with the force moving from left to right at a constant speed c, as shown in Figure 2, the equation of motion can be written as

$$\rho \frac{\partial^2 v(x,t)}{\partial t^2} + C \frac{\partial v(x,t)}{\partial t} + EI \frac{\partial^4 v(x,t)}{\partial x^4} = \delta(x - ct) f(t), \tag{3}$$

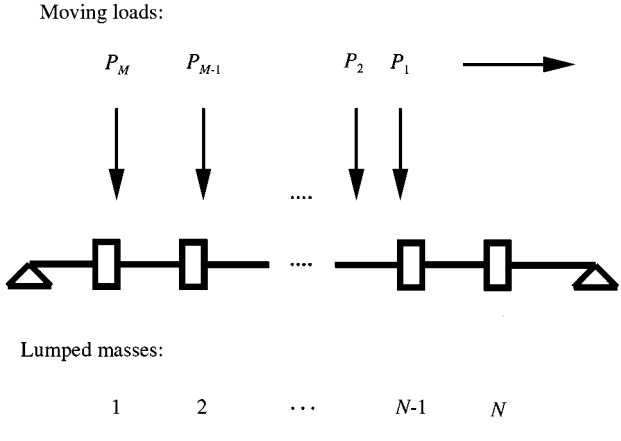

Figure 1. Beam–element model.

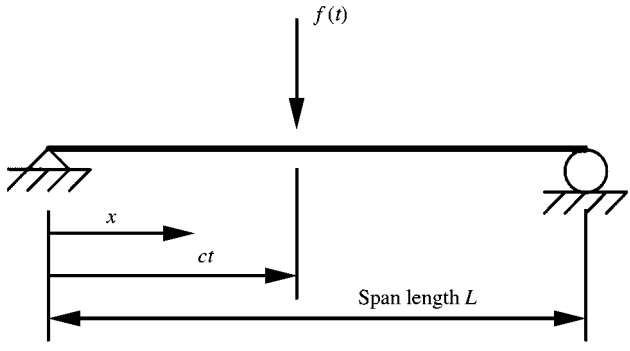

Figure 2. Simply supported beam subjected to a moving force $f(t)$.

where $v(x, t)$ is the beam deflection at point x and time t; ρ is the mass per unit length; C is the viscous damping parameter; E is Young's modulus of the material: I is the moment of inertia of the beam cross-section; $f(t)$ is the time-varying force moving at a constant speed of c, and $\delta(t)$ is the Dirac delta function.

Based on modal supersposition, the dynamic deflection $v(x, t)$ can be described as follows:

$$v(x, t) = \sum_{n=1}^{\infty} \phi_n(x) q_n(t), \tag{4}$$

where n is the mode number; $\phi_n(x)$ is the mode shape function of the nth mode, and $q_n(t)$ gives the nth modal amplitude.

3. THEORETICAL BACKGROUND OF MFIM

Based on these methods of predictive analysis, four moving force identification methods have been developed.

3.1. INTERPRETIVE METHOD I—BEAM-ELEMENT MODEL (IMI)

This is the inverse problem to the predictive beam-element model analysis. From equation (1), it can be seen that if Y is known at all times for all interior nodes, then $\dot{Y}$ and $\ddot{Y}$ can be obtained using a numerical differentiation method. Equation (1) becomes an over-determined set of linear simultaneous equations from which P may be solved. However, a particular difficulty arises if measured bending moments are used as input data. Remembering that the moving loads P are not normally at the nodes, the relation between the nodal displacements and the nodal bending moments is

$$\{Y\} = [Y_B]\{M\} + [Y_C]\{P\}, \tag{5}$$

where $[Y_B]$ and $[Y_C]$ are separate matrices for nodal bending moments and the applied forces. $[Y_C]\{P\}$ allows for the deflections due to the additional triangularly distributed bending moment, which occurs within elements carrying one or more point loads P. $[Y_C]$ can be calculated from the known locations of the loads $[Y_B]$ and $\{M\}$ are known, but $\{Y\}$ cannot be determined without a knowledge of $\{P\}$. O'Connor and Chan [6] describe a solution that uses values of $\{P\}$ assumed from the previous time steps.

3.2. INTERPRETIVE METHOD II—CONTINUOUS BEAM MODEL (IMII)

From the predictive analysis using the continuous beam model, if the ith mode shape function of the simply supported Euler beam is assumed as $\sin i\pi x/L$, then the solution of equation (3) takes the form

$$v = \sum_{i=1}^{\infty} \sin \frac{i\pi x}{L} q_i(t), \tag{6}$$

where $q_i(t)$, $(i = 1, 2, \dots)$ are the modal displacements.

Substituting equation (6) into equation (3), and multiplying each term of equation (3) by the mode shape function $\sin j\pi x/L$, and then integrating the resultant equation with respect to x between 0 and L using the boundary conditions and the Dirac function properties, the following equation can be obtained:

$$\ddot{q}_j(t) + 2\xi_j \omega_{(j)} \dot{q}_j(t) + \omega_{(j)}^2 q_j(t) = \frac{2P}{\rho L} \sin j\omega t, \quad j = 1, 2, \dots \tag{7}$$

$$\text{where } \omega_{(j)}^2 = \frac{j^4\pi^4}{L^4} \frac{EI}{\rho} \quad \text{and} \quad \xi_{(j)} = \frac{C}{2\rho\omega_{(j)}} \text{ at the } j\text{th mode.}$$

If there is more than one moving load on the beam, equation (7) can be written as

$$\begin{bmatrix} \ddot{q}_1 \\ \ddot{q}_2 \\ \vdots \\ \ddot{q}_n \end{bmatrix} + \begin{bmatrix} 2\xi_1\omega_1\dot{q}_1 \\ 2\xi_2\omega_2\dot{q}_2 \\ \vdots \\ 2\xi_n\omega_n\dot{q}_n \end{bmatrix} + \begin{bmatrix} \omega_1^2 q_1 \\ \omega_2^2 q_2 \\ \vdots \\ \omega_n^2 q_n \end{bmatrix}$$

$$= \frac{2}{\rho L} \begin{bmatrix} \sin \dfrac{\pi(ct - \hat{x}_1)}{L} & \sin \dfrac{\pi(ct - \hat{x}_2)}{L} & \cdots & \sin \dfrac{\pi(ct - \hat{x}_k)}{L} \\ \sin \dfrac{2\pi(ct - \hat{x}_1)}{L} & \sin \dfrac{2\pi(ct - \hat{x}_2)}{L} & \cdots & \sin \dfrac{2\pi(ct - \hat{x}_k)}{L} \\ \vdots & \vdots & \vdots & \vdots \\ \sin \dfrac{n\pi(ct - \hat{x}_1)}{L} & \sin \dfrac{n\pi(ct - \hat{x}_2)}{L} & \cdots & \sin \dfrac{n\pi(ct - \hat{x}_k)}{L} \end{bmatrix} \begin{bmatrix} P_1 \\ P_2 \\ \vdots \\ P_k \end{bmatrix} \tag{8}$$

in which $\hat{x}_k$ is the distance between the kth load and the first load and $\hat{x}_1 = 0$.

If $P_1, P_2, \dots, P_k$ are constants, the closed-form solution of equation (3) is

$$v(x, t) = \frac{L^3}{48EI} \sum_{i=1}^{k} P_i \sum_{j=1}^{\infty} \frac{1}{j^2(j^2 - \alpha^2)} \sin \frac{j\pi x}{L} \left(\sin \frac{j\pi(ct - \hat{x}_i)}{L} - \frac{\alpha}{j} \sin \omega_{(j)} \left(t - \frac{\hat{x}_i}{c} \right) \right) \tag{9}$$

in which $\alpha = \pi c/L\omega$.

If we know the displacements of the beam at $x_1, x_2, \dots, x_l$, the moving loads on the beam are given by

$$\{v\} = [S_{vp}]\{P\} \tag{10}$$

in which $\{v\} = [v_1 \ v_2 \ \cdots \ v_l]^T$, $\{P\} = [P_1 \ P_2 \ \cdots \ P_k]$,

$$[S_{vp}] = \begin{bmatrix} s_{11} & \cdots & \cdots & \cdots & s_{1k} \\ \vdots & \ddots & & & \vdots \\ s_{m1} & & s_{mi} & & s_{mk} \\ \vdots & & & \ddots & \vdots \\ s_{l1} & \cdots & \cdots & \cdots & s_{lk} \end{bmatrix}, \text{ where}$$

$$s_{mi} = \frac{L^3}{48EI} \sum_{j=1}^{\infty} \frac{1}{j^2(j^2 - \alpha^2)} \sin \frac{j\pi x_m}{L} \left(\sin \frac{j\pi(ct - \hat{x}_i)}{L} - \frac{\alpha}{j} \sin \omega_{(j)} \left(t - \frac{\hat{x}_i}{c} \right) \right).$$

If $l \geqslant k$, that means the number of nodal displacements is larger than or equal to the number of axle loads, and the equivalent static axle load can be obtained using the least-squares methods,

$$\{P\} = ([S_{vp}]^T [S_{vp}])^{-1} [S_{vp}]^T \{v\}. \tag{11}$$

If the loads are not constant with time, then the central difference method is used to find modal velocities and accelerations from the modal displacements. Equation (8) becomes a set of linear equations in which P_k for any instant can be solved by the least-squares method. Similar sets of equations could be obtained based on the use of bending moments to identify the moving loads [7].

3.3. SYSTEM IDENTIFICATION I—TIME DOMAIN METHOD (TDM)

This method is based on the system identification theory [8]. Substituting equation (4) into equation (3), multiplying each term by $\phi_j(x)$, then integrating with respect to x between 0 and L, and applying the orthogonality conditions,

$$\frac{d^2 q_n(t)}{dt^2} + 2\xi_n \omega_n \frac{dq_n(t)}{dt} + \omega_n^2 q_n(t) = \frac{1}{M_n} p_n(t), \tag{12}$$

where ω_n is the circular natural frequency of the nth mode; ξ_n is the dampling ratio of the nth mode; M_n is the modal mass of the nth mode; $p_n(t)$ is the modal force, and the mode shape function can be assumed as $\phi_n(x) = \sin n\pi x/L$.

Equation (12) can be solved in the time domain by the convolution integral, yielding

$$q_n(t) = \frac{1}{M_n} \int_0^t h_n(t - \tau)\, p(\tau)\, d\tau, \tag{13}$$

$$\text{where } h_n(t) = \frac{1}{\omega_n'} e^{-\xi_n \omega_n t} \sin(\omega_n' t), \quad t \geqslant 0 \tag{14}$$

$$\text{and } \omega_n' = \omega_n \sqrt{1 - \xi_n^2} \tag{15}$$

Substituting equation (13) into equation (4), the dynamic deflection of the beam at point x and time t can be found as

$$v(x, t) = \sum_{n=1}^{\infty} \frac{2}{\rho L \omega_n'} \sin \frac{n\pi x}{L} \int_0^t e^{-\xi_n \omega_n (t - \tau)} \sin \omega_n'(t - \tau) \sin \frac{n\pi c\tau}{L} f(\tau)\, d\tau. \tag{16}$$

3.3.1. *Force identification from bending moments*

The bending moment in the beam at point x and time t is

$$m(x, t) = -EI \frac{\partial^2 v(x, t)}{\partial x^2}. \tag{17}$$

Substituting equation (16) into equation (17), and assuming the force $f(t)$ is a step function over a small time interval and $f(t) = 0$ at entry and exit,

$$C_{xn} = \frac{2EI\pi^2}{\rho L^3} \frac{n^2}{\omega_n'} \sin \frac{n\pi x}{L} \Delta t, \tag{18}$$

$$E_n^k = \mathrm{e}^{-\xi_n \omega_n \Delta t k},$$

$$S_1(k) = \sin(\omega_n' \Delta t k), \tag{19}$$

$$S_2(k) = \sin\left(\frac{n\pi c \Delta t}{L} k\right) \text{ and}$$

$$N_B = \frac{L}{c\Delta t}.$$

Equation (17) can be expressed as

$$\begin{Bmatrix} m(2) \\ m(3) \\ \vdots \\ m(N) \end{Bmatrix} = \sum_{n=1}^{\infty} C_{xn} \begin{bmatrix} E_n^1 S_1(1) S_2(1) & 0 & \cdots & 0 \\ E_n^2 S_1(2) S_2(1) & E_n^1 S_1(1) S_2(2) & \cdots & 0 \\ \vdots & \vdots & \vdots & \vdots \\ E_n^{N-1} S_1(N-1) S_2(1) & E_n^{N-2} S_1(N-2) S_2(2) & \cdots & b_{ec} \end{bmatrix} \begin{Bmatrix} f(1) \\ f(2) \\ \vdots \\ f(N_B - 1) \end{Bmatrix}, \tag{20}$$

where Δt is the sampling interval and $N + 1$ is the number of sample points, and

$$b_{ee} = E_n^{N-N_B+1} S_1(N - N_B + 1) S_2(N_B - 1).$$

Equation (20) can be simplified as

$$\underset{(N-1)\times(N_B-1)}{B} \quad \underset{(N_B-1)\times 1}{f} = \underset{(N-1)\times 1}{m}. \tag{21}$$

If $N = N_B$, matrix B is a lower triangular matrix. We can directly find the force vector f by solving equation (21). If $N > N_B$, and/or N_l bending moments ($N_l > 1$) are measured, using the least-squares method to find the force vector f from

$$\begin{bmatrix} B_1 \\ B_2 \\ \vdots \\ B_{N_l} \end{bmatrix} \{f\} = \begin{Bmatrix} m_1 \\ m_2 \\ \vdots \\ m_{N_l} \end{Bmatrix}. \tag{22}$$

The above procedure is applied only to single force identification. Equation (21) can be modified for two-force identification purpose using the linear superposition principle expressed as

$$\begin{bmatrix} B_a & 0 \\ B_b & B_a \\ B_c & B_b \end{bmatrix} \begin{Bmatrix} f_1 \\ f_2 \end{Bmatrix} = \{m\}, \tag{23}$$

where $B_a[N_s \times (N_B - 1)]$, $B_b[(N - 1 - 2N_s) \times (N_B - 1)]$, and $B_c[N_s \times (N_B - 1)]$ are sub-matrices of matrix B; $N_s = l_s/c\Delta t$, and l_s is an axle spacing. The first row of sub-matrices in the first matrix describes the state when only the first force has affected the beam. The second and third rows of sub-matrices describe, respectively, the states when there are two forces on the beam and when the second force remains on the beam after the exit of the first force.

3.3.2. *Force identification from bending moments and accelerations*

Similarly the acceleration response of the beam can be expressed as

$$\underset{N \times (N_B - 1)}{A} \quad \underset{(N_B - 1) \times 1}{f} = \underset{N \times 1}{\ddot{v}}. \tag{24}$$

The force acting can also be found from the measured acceleration from equation (24). If the bending moment and acceleration responses are measured at the same time, both of them can be used together to identity the moving force. The vector m in equation (21) and $\ddot{v}$ in equation (24) should be scaled to make them dimensionless, and the two equations are then combined to give

$$\begin{bmatrix} B/\|m\| \\ A/\|\ddot{v}\| \end{bmatrix} \{f\} = \begin{Bmatrix} m/\|m\| \\ \ddot{v}/\|\ddot{v}\| \end{Bmatrix}, \tag{25}$$

where $\|\bullet\|$ is the norm of the vector.

3.4. SYSTEM IDENTIFICATION II—FREQUENCY–TIME DOMAIN METHOD (FTDM)

Equation (12) can also be solved in the frequency domain. Performing the Fourier transform for equation (12),

$$Q_n(\omega) = \frac{1}{\omega_n^2 - \omega^2 + 2\xi_n\omega_n\omega} \frac{1}{M_n} P_n(\omega), \tag{26}$$

where

$$P_n(\omega) = \frac{1}{2\pi} \int_{-\infty}^{\infty} p_n(t)\, \mathrm{e}^{-\mathrm{i}\omega t}\, \mathrm{d}t \tag{27}$$

and

$$Q_n(\omega) = \frac{1}{2\pi} \int_{-\infty}^{\infty} q_n(t)\, \mathrm{e}^{-\mathrm{i}\omega t}\, \mathrm{d}t \tag{28}$$

$$\text{Letting } H_n(\omega) = \frac{1}{\omega_n^2 - \omega^2 + 2\xi_n\omega_n\omega}, \tag{29}$$

where $H_n(\omega)$ is the frequency response function of the nth mode, performing the Fourier transform of equation (4), and substituting equations (26) and (29) into the resultant equation, the Fourier transform of the dynamic deflection $v(x, t)$ is obtained as

$$V(x, \omega) = \sum_{n=1}^{\infty} \frac{1}{M_n} \phi_n(x) H_n(\omega) P_n(\omega). \tag{30}$$

3.4.1. *Force identification from accelerations*

Based on equation (30), the Fourier transform of the acceleration of the beam at point x and time t can be written as

$$\ddot{V}(x, \omega) = -\omega^2 \sum_{n=1}^{\infty} \frac{1}{M_n} \phi_n(x) H_n(\omega) P_n(\omega). \tag{31}$$

Considering the periodic property of the discrete Fourier transform (DFT), and letting

$$\bar{H}_{xn}(m) = -\frac{\Delta f^3 m^2}{M_n} \phi_n(x) H_n(m). \tag{32}$$

Equation (32) can be written as

$$\begin{aligned}
\ddot{V}(m) = & \sum_{n=1}^{\infty} \bar{H}_{xn}(m) \psi_n(m) [F_R(0) + iF_I(0)] \\
& + \sum_{k=1}^{N/2-1} \sum_{n=1}^{\infty} \bar{H}_{xn}(m) [\psi_n(m-k) + \psi_n(m+k-N)] F_R(k) \\
& + i \sum_{k=1}^{N/2-1} \sum_{n=1}^{\infty} \bar{H}_{xn}(m) [\psi_n(m-k) - \psi_N(m+k-N)] F_I(k), \quad m = 0, 1, \ldots, N-1 \\
& + \sum_{n=1}^{\infty} \bar{H}_{xn}(m) \psi_n(m - N/2) [F_R(N/2) - iF_I(N/2)],
\end{aligned} \tag{33}$$

where ψ_n is the Fourier transform of the nth mode shape, and F is the Fourier transform of the moving force.

Writing equation (33) into matrix form and dividing F and $\ddot{v}$ into real and imaginary parts, yields

$$\underset{(N+2)\times 1}{\begin{Bmatrix} \ddot{V}_R \\ \ddot{V}_I \end{Bmatrix}} = \underset{(N+2)\times(N+2)}{\begin{bmatrix} A_{RR} & -A_{II} \\ A_{RI} & A_{IR} \end{bmatrix}} \underset{(N+2)\times 1}{\begin{Bmatrix} F_R \\ F_I \end{Bmatrix}}. \tag{34}$$

Because $F_I(0) = 0$, $F_I(\frac{N}{2}) = 0$, $\ddot{V}_I(0) = 0$, $\ddot{V}_I(\frac{N}{2}) = 0$, equation (34) can be condensed into a set of N order simultaneous equations as

$$\ddot{V}_{RI} = A_D F_{RI}. \tag{35}$$

F_R and F_I can be found from equation (35) by solving the Nth order linear equations. The time history of the moving force $f(t)$ can then be obtained by performing the inverse Fourier transformation.

If the DFTs are expressed in matrix form, the Fourier transform of the force vector f can be written as follows if the terms in f are real [9]:

$$F = \frac{1}{N} Wf, \tag{36}$$

where

$$W = \mathrm{e}^{(-\mathrm{i}2k\pi/N)},$$

$$k = \begin{bmatrix} 0 & 0 & 0 & \cdots & 0 & 0 \\ 0 & 1 & 2 & \cdots & N-2 & N-1 \\ 0 & 2 & 4 & \cdots & N-4 & N-2 \\ \vdots & \vdots & \vdots & & \vdots & \vdots \\ 0 & N-2 & N-4 & \cdots & 4 & 2 \\ 0 & N-1 & N-2 & \cdots & 2 & 1 \end{bmatrix}_{N\times N}. \tag{37}$$

The matrix W is a unitary matrix, which means

$$W^{-1} = (W^*)^{\mathrm{T}}, \tag{38}$$

where W^* is a conjugate of W. Substituting equation (36) into equation (35),

$$\ddot{V} = \frac{1}{N} A \begin{bmatrix} W_B & 0 \\ {\scriptstyle N\times N_B} & \end{bmatrix} \begin{Bmatrix} f_B \\ 0 \end{Bmatrix} \tag{39}$$

or

$$\underset{N\times 1}{\ddot{V}} = \frac{1}{N} \underset{N\times N}{A}\ \underset{N\times N_B}{W_B}\ \underset{N_B\times 1}{f_B} \tag{40}$$

linking the Fourier transform of acceleration $\ddot{V}$ with the force vector f_B of the moving forces in the time domain. W_B is the sub-matrix of W. If $N = N_B, f_B$ can be found by solving the Nth order linear equations. If $N > N_B$ or more than one acceleration is measured, the least-squares method can be used to find the time history of the moving force $f(t)$.

Equation (40) can be written as follows:

$$\underset{N\times 1}{\ddot{v}} = \underset{N\times N}{(W^*)^{\mathrm{T}}}\ \underset{N\times N}{A}\ \underset{N\times N_B}{W_B}\ \underset{N_B\times 1}{f_B}, \tag{41}$$

relating the accelerations and force vectors in the time domain. Also if $N = N_B, f_B$ can be found by solving the Nth order linear equations. If $N > N_B$ or more than one acceleration is measured, the least-squares method can be used to find the time history of the moving force $f(t)$.

If only $N_C (N_C \leqslant N)$ response data points on the beam are used, the equations for these data points in equation (41) are extracted, and described as

$$\underset{N_C\times 1}{\ddot{v}_c} = \underset{N_C\times N}{(W_B^*)^{\mathrm{T}}}\ \underset{N\times N}{A}\ \underset{N\times N_B}{W_B}\ \underset{N_B\times 1}{f_B}. \tag{42}$$

Usually $N_C > N_B$, so the least-squares method is used to find the time history of the moving force $f(t)$. For higher accuracy, acceleration measurements at different locations can be used together to identify a single moving force.

3.4.2. *Identification from bending moments and accelerations*

Similarly, the relationships between bending moment m (and M) and the moving force f can be described as follows:

$$\underset{N\times 1}{M} = \frac{1}{N}\,\underset{N\times N}{B}\,\underset{N\times N_B}{W}\,\underset{N_B\times 1}{f_B}, \tag{43}$$

$$\underset{N\times 1}{m} = \underset{N\times N}{(W^*)^{\mathrm{T}}}\,\underset{N\times N}{B}\,\underset{N\times N_B}{W_B}\,\underset{N_B\times 1}{f_B}, \tag{44}$$

$$\underset{N_C\times 1}{m_B} = \underset{N_C\times N}{(W^*)^{\mathrm{T}}}\,\underset{N\times N}{B}\,\underset{N\times N_B}{W_B}\,\underset{N_B\times 1}{f_B}. \tag{45}$$

The force vector f_B can be obtained from the above three sets of equations. These equations can also be combined with equations (40)–(42) to construct over-determined equations before the equations are scaled. Two forces are identified using a procedure similar to that for the time domain method.

In the formulation shown above, the governing equations are initially formulated in the frequency domain. The solution, however, is obtained in the time domain, and the method is therefore called the frequency–time domain method [10].

4. IMPLEMENTATION

4.1. INTERPRETIVE METHOD I (IMI) AND INTERPRETIVE METHOD II (IMII)

Two FORTRAN programs have been developed separately based on the two interpretive methods, IMI and IMII. Each programme consists of two sections. The first section is based on the corresponding predictive analysis to simulate the dynamic responses caused by a set of moving loads. The other provides force identification by deducing the values of the moving loads from the simulated responses. This section serves to check whether the moving force identification methods can recover the original set of moving loads. In the simulation process, a set of ordinary differential equations (equations (1–3)) is solved to obtain the dynamic responses at the corresponding locations. Newmark's method and the Runge–Kutta method are adopted as the solution routines for the programs IMI and IMII respectively. Two types of dynamic responses—displacements and bending moments,—which can be easily checked from the closed-form solution, are selected as the output data. For the force identification part, both programs IMI and IMII require bending moments as the input data because bending moments are easier to acquire using strain guages. The measured bending moments are then converted to displacements, velocities, and accelerations. The central difference method is adopted for calculating the velocities and accelerations from displacements for both the IMI and IMII cases. An equivalent force is then calculated from the sum of the inertia force, damping force and static force. The equivalent force is then multiplied by an influence matrix to obtain the identified force. There are two influence matrices. The first is the matrix $[M_A]$ in equation (2) for the IMI case. The second is the load vector multiplication matrix in equation (8) for the IMII case. As the number of measuring nodes may not be equal to the number of axles, the least-squares method is used to solve the over-determined set of equations.

4.2. TIME DOMAIN METHOD (TDM) AND FREQUENCY–TIME DOMAIN METHOD (FTDM)

As TDM and FTDM involve a number of numerical functions and such functions are built standard functions in MATLAB [11], for convenience, two MATLAB programs have

TABLE 1

Summary of the sensor arrangement for TDM and FTDM

	Case											
	i	ii	iii	iv	v	vi	vii	viii	ix	x	xi	xii
$\frac{1}{4}$a			o	o			o	o	o	o	o	o
$\frac{1}{2}$a			o	o	o	o	o		o			o
$\frac{3}{4}$a				o								
$\frac{1}{4}$m	o	o				o	o	o	o		o	
$\frac{1}{2}$m	o	o			o	o	o			o	o	o
$\frac{3}{4}$m		o										

Note: o—sensor location, a—using accelerometers, m—using strain gauges; $\frac{1}{4}$, $\frac{1}{2}$, $\frac{3}{4}$—quarter, mid, three-quarter span respectively.

been developed based on the two system identification methods. Relating to both IMI and IMII methods, each programme consists of two sections. The first is based on the corresponding predictive analysis to simulate the dynamic responses caused by a set of moving loads and the other is to identify the values of the moving loads from the simulated responses. As the number of measuring nodes may not be equal to the number of axles, the least-squares method is also used to solve for the over-determined set of equations.

MATLAB requires a large amount of computer memory for the inversion of a large matrix. Because of this the developed TDM and FTDM have three limitations. For both systems, the maximum number of identifiable axles under the MATLAB environment is limited to two. The second limitation is the location of sensors. At present only 12 combinations of sensor arrangement have been developed with a maximum of four sensors (case vii) as shown in Table 1. In Table 1, 1/4a, 1/2a, or 3/4a indicate having an accelerometer at quarter-span, mid-span, or three-quarter span respectively. Similarly, 1/4m, 1/2m or 3/4m indicate having a strain guage at quarter-span, mid-span, or three-quarter span respectively. The last limitation is that both TDM and FTDM require a minimum amount of memory in hard disk and RAM (Read Access Memory) of 150 and 16 MB respectively.

5. PRACTICAL APPLICATION

Moving loads on structures cause larger responses than static loads. A ratio of the maximum dynamic response to the corresponding static response is defined as an impact factor or a dynamic amplification factor [12]. The impact factor can be obtained from field tests on highway bridges. In practical measurement, strain guages and accelerometers are commonly used to acquire strains for bending moments, and displacements for accelerations respectively. The measured response–time history can then be used to determine the impact factor. In this study, the measured response–time history has been used for the force identification based on the identified force–time history. The force–time history is then converted into the frequency domain using fast Fourier transform as the force–frequency spectrum. The force–frequency spectrum can be used to study the effect of vehicles on a bridge, providing a better understanding of bridge vehicle interaction.

6. EXAMPLES

Four cases are studied, namely, case i—constant force identification, case ii—time-varying force identification, case iii—constant force identification with noise added and case iv—time-varying force identification with noise added. The bridge model has a span length of 40 m, a flexural stiffness of $1{\cdot}27914 \times 10^{11}$ Nm^2, and a unit mass of 12000 kg/m. The vehicle model travelling at a speed of 40 m/s has an axle spacing of 8 m with the first and second static axle forces being 58·8 and 137·2 KN respectively. For the time-varying force identification, both the first and second axle forces oscillate about their mean values in phase within an amplitude range of 20% of the mean. For the IMI and IMII cases, seven equally spaced locations along the bridge model were chosen to generate bridge responses as the input data. For the TDM and FTDM cases, the arrangement of sensors is as shown in Table 1.

In the present study, a percentage error is used to express the difference between the true and the identified axle forces. The percentage error is defined as a ratio of the sum of the absolute value of the difference between the true and identified axle forces to the sum of the absolute value of the true axle force or, equivalently,

$$\varepsilon_{error} = \frac{\sum |\varepsilon_{true} - \varepsilon_{ident}|}{\sum |\varepsilon_{true}|} \times 100\% \tag{46}$$

where ε_{error} is the percentage error; ε_{true} is the true value, and ε_{ident} is the identified value.

A summary of the percentage errors of the four examples is tabulated in Table 2. Table 2 shows that the percentage errors for the four identification methods are less then 2% when the responses are not contaminated. The results also show that TDM and FTDM are the best methods for identification of moving forces because both methods produce the least percentage errors on constant and time-varying moving force identification when responses are not contaminated. Figure 3 shows typical identified axle forces without consideration of contamination in the responses using the four identification methods.

Table 2 and Figure 3 show that IMI and IMII could not obtain zero percentage errors on the above examples even when the level of noise is 0%. This is because the velocities and accelerations obtained in the force identification are different from the velocities and accelerations obtained in the simulation using different solution methods. In the simulation, Newmark's method and the Runge–Kutta method are adoped in IMI and IMII, respectively; however, the central difference method is adopted in the force identification. Despite IMI and IMII having the highest percentage errors, the magnitude of the errors is

TABLE 2

A summary of the percentage errors of the moving force identification study

	Percentage error (%)							
	IMI		IMII		TDM		FTDM	
Case	Axle 1	Axle 2	Axle 1	Axle 2	Axle 1	Axle 2	Axle 1	Axle 2
i	1·3	0.8	1·6	1·7	0·0	0·0	0·0	0·0
ii	1·2	0·8	1·6	1·9	0·0	0·0	0·0	0·0
iii (with 5% noise)	176·8	81·8	52·4	24·2	4·2	4·3	9·3	6·9
iv (with 5% noise)	177·4	81·6	52·2	24·2	4·5	4·7	8·9	6·5

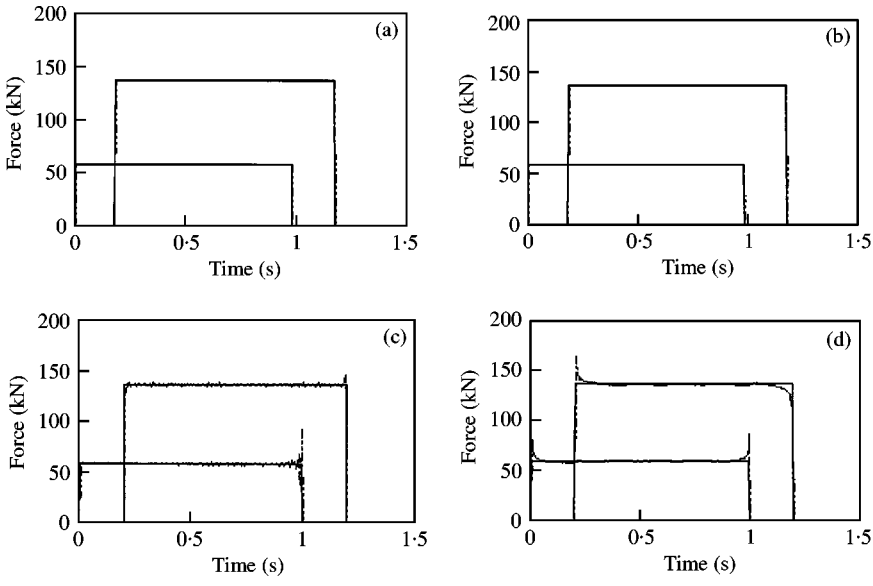

Figure 3. Typical identified constant axle forces using the four identification methods. —, True axle force; _·_·_·_, Identified axle force. Typical identified axle forces using (a) TDM, (b) FTDM, (c) IMI, (d) IMII.

TABLE 3

A summary of the percentage errors of the filtered axle forces

	Percentage error (%)			
	IMI		IMII	
Case	Axle 1	Axle 2	Axle 1	Axle 2
iii (with 5% noise)	10·6	7·8	5·8	4·9
iv (with 5% noise)	11·7	9·3	7·5	7·4

small enough to be ignored, and therefore both IMI and IMII are also applicable for moving force identification.

The results of using TDM and FTDM show that case iv gives excellent results. The percentage errors of case iv of both TDM and FTDM are shown in Table 2. It can be seen that IMI and IMII produce large percentage errors, indicating they are sensitive to noise. Therefore, it is interesting to study whether the results can be improved using a low-pass filter. Results of the filtered axle forces are tabulated in Table 3. Typical filtered identified constant and time-varying axle forces with 5% noise are shown in Figures 4 and 5 respectively.

Table 3 shows that the results of IMII after filtering have percentage errors less than 10%. The results of IMI after filtering have percentage errors greater than 10% for the first axle but can still be considered fairly acceptable.

It may be concluded from above illustrative examples that the four identification methods are applicable for the force identification of constant and time-varying forces. A detailed study on the comparative merits and limitations of the four moving force identification methods is presented in the accompanying report [13].

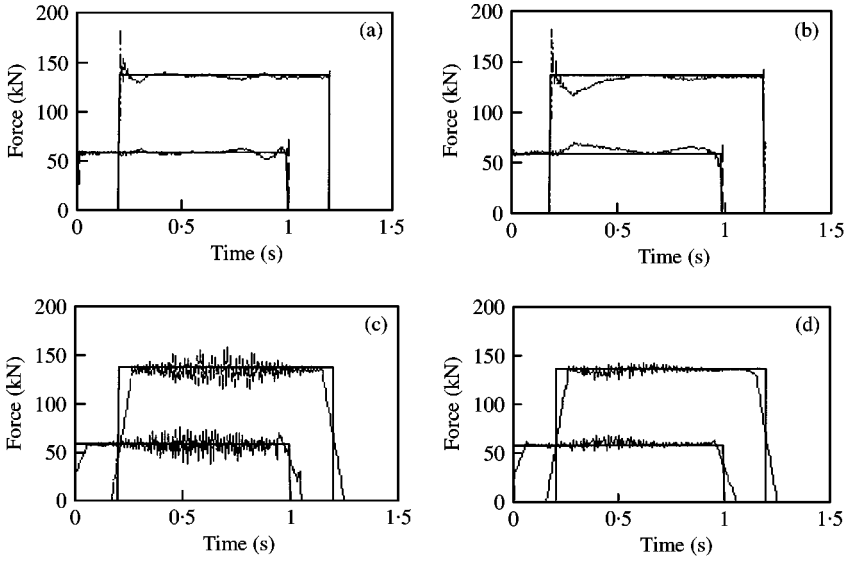

Figure 4. Typical identified constant axle forces with 5% noise using the four identification methods. —, True axle force; _..._..., Identified axle force. Typical identified axle forces using (a) TDM, (b) FTDM, (c) IMI, (d) IMII.

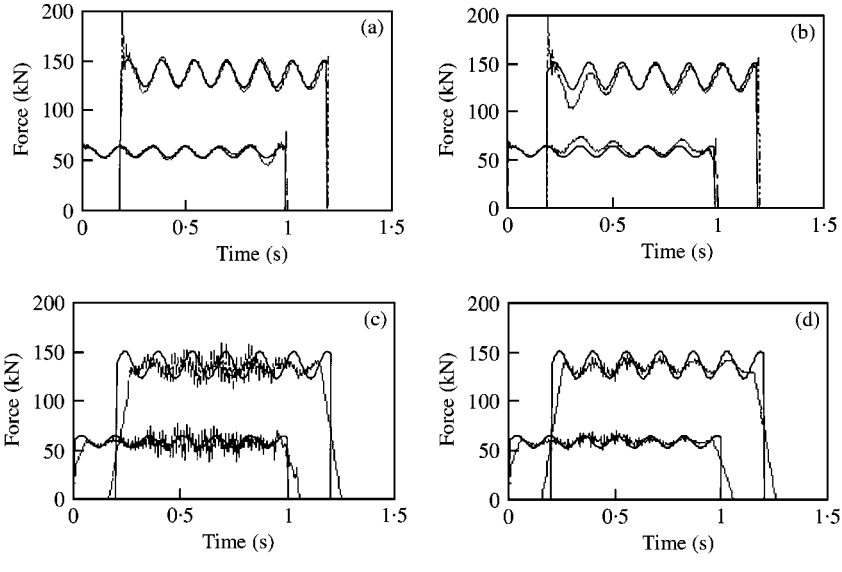

Figure 5. Typical identified time-varying forces with 5% noise using the four identification methods. —, True axle force; _..._..., Identified axle force. Typical identified axle forces using (a) TDM, (b) FTDM, (c) IMI, (d) IMII.

7. EXPERIMENTAL VALIDATION

To further validate the feasibility of the four identification methods, a series of experiments have been conducted in the laboratory. Both the model car and model bridge deck were constructed in the laboratory. An axle-spacing-to-span-ratio (ASSR) is defined as the ratio of the axle spacing between two consecutive axles of the vehicle to the bridge span

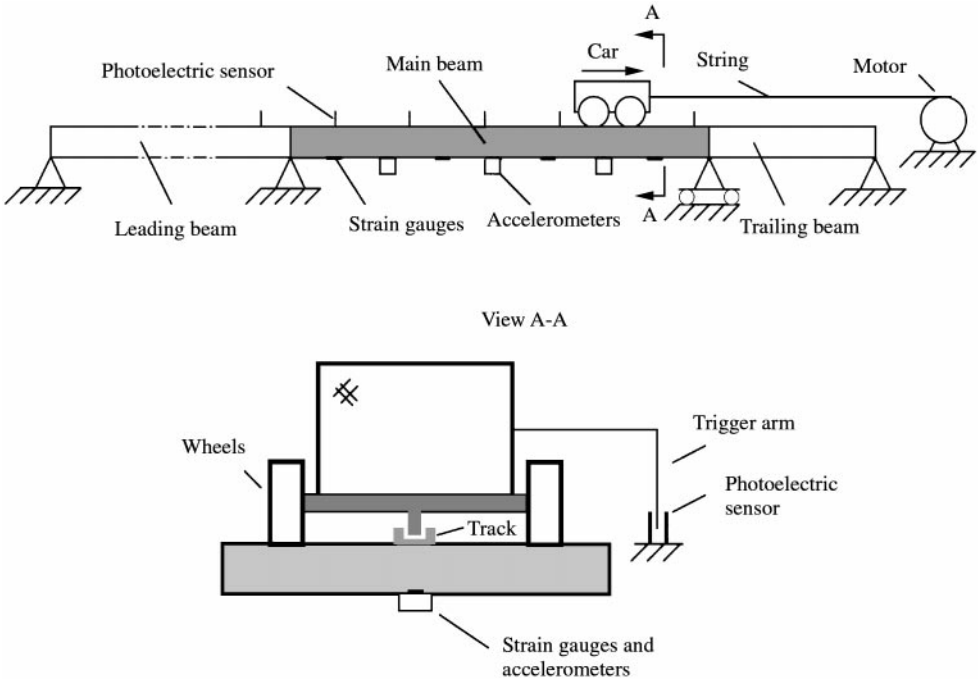

Figure 6. Experimental setup of moving force identification.

length. Here, the ASSR was set to be 0·15. The model car had two axles at a spacing of 0·55 m and was mounted on four rubber wheels. The static mass of the whole vehicle was 12·1 kg in which the mass of the rear wheels was 3·825 kg. The model bridge deck consisted of a main beam, a leading beam and a trailing beam as shown in Figure 6. On the leading beam a constant vehicle speed was reached as the model car approached the bridge. The trailing beam was used for decelerating the car. The main beam with a span of 3·678 m length and 101 mm × 25 mm uniform cross-section was simply supported. It was made from a solid rectangular mild steel bar with a density of 7335 kg/m^3 and a flexural stiffness $EI = 29{\cdot}97$ kN/m^2. The first three theoretical natural frequencies of the main beam bridge were calculated as $f_1 = 4{\cdot}5$ Hz, $f_2 = 18{\cdot}6$ Hz and $f_3 = 40{\cdot}5$ Hz.

A U-shaped aluminium track was glued to the upper surface of the main beam as a guideway for the model car, which was pulled along by a string wound around the drive wheel of an electric motor. The speed of the motor could be adjusted. Three different car speeds were set at 5, 10 and 15 Units (1 Unit $\cong 0{\cdot}102$ m/s). Seven photoelectric sensors were mounted on the beams to measure and check the uniformity of the moving speed of the model car. Seven equally spaced strain guages and three equally spaced accelerometers were mounted on the lower surface of the main beam to measure the response. A system calibration of the strain guages was carried out before the actual testing program by adding masses at the middle of the main beam. A 14-channel tape recorder was employed to record the response signals. The first seven channels were used for logging the bending moment response signals from the strain guages. Channels 8–10 were used for logging the accelerations from the accelerometers. Channel 11 was connected to the photoelectric sensors. The software Global Lab from the Data Translation was used for data acquisition and analysis in the laboratory test. Before exporting the measured data in ASCII format for identification, the Bessel IIR digital filter with low-pass characteristics

TABLE 4

A summary of the percentage errors for experimental case

Method	Percentage error (%)						
	Sta.1	Sta.2	Sta.3	Sta.4	Sta.5	Sta.6	Sta.7
IMI	7·16	6·07	5·99	5·46	5·13	4·78	4·50
IMII	15·97	9·46	8·26	5·13	6·95	8·64	16·59
TDM	5·91	3·32	1·92	2·79	1·96	3·68	5·77
FTDM	5·83	3·32	1·88	2·80	1·92	3·69	5·73

was implemented as cascaded second order systems. The Nyquist fraction value was chosen to be 0·03.

Under different experimental conditions, both the bending moments and accelerations have been measured simultaneously when the vehicle moves across the bridge at different speeds. After the moving axle loads were identified from these measured responses based on the four identification methods, respectively, the rebuilt responses were then calculated from these identified loads and the percentage errors between the rebuilt and the measured responses were evaluated according to equation (46). Here, the measured response ($R_{measured}$) and rebuilt response ($R_{rebuilt}$) are substituted for the true force (ε_{true}) and identified force (ε_{ident}) respectively. A summary of the percentage errors of the four identification methods is tabulated in Table 4. The case corresponds to the second set of a total of five records under 15 Units. Where the car speed is 15 Units, the sampling frequency is 333·33 Hz. The mode numbers involved in the identification calculation are 3 for IMII and 4 for both TDM and FTDM respectively. Only seven measured bending moments were used, in which each one has 930 data samples in the time domain.

Table 4 shows that all the four identification methods can effectively identify the two moving axle loads and both TDM and FTDM have good identification accuracy. A detailed laboratory study on the comparative merits and limitations of the four moving force identification methods was carried out [14] and some of the results are presented in the accompanying paper [13].

8. CONCLUSIONS

An introduction to four moving force identification methods has been given. The computer implementation of the four moving force identification methods has also been briefly described and some application examples are given. The illustrative examples and experiments in the laboratory show that all the four identification methods are valid for the identification of moving forces on a simply supported beam. It also shows that IMI and IMII are more sensitive to noise effects and the use of a low-pass filter is recommended to obtain filtered identified forces. A detailed comparative study of the four moving force identification methods is given in a separate report.

ACKNOWLEDGMENTS

This project is funded by the Research Grants Council of the Hong Kong Government.

REFERENCES

1. P. DAVIS and F. SOMMERVILLE 1986 *Proceedings of the 13th ARRB & 5th REAAA Combined Conference*, Australia Part 6, 142–149. Low-cost axle load determination.
2. R. J. PETERS 1984 *Proceedings of 12th ARRB Conference*, Australia **12**(2), 10–18. A system to obtain vehicle axle weights.
3. R. J. PETERS 1986 *Proceedings of 13th ARRB and 5th REAAA Combined Conference*, Australia Part 6, 70–83. An unmanned and undetectable highway speed vehicle weighing system.
4. D. CEBON 1987 *Symposium on Heavy Vehicle Suspension Characteristics*, *ARRB*, Australia. Assessment of the dynamic wheel forces generated by heavy vehicle road vehicles.
5. R. CANTIENI 1992 *Swiss Federal Laboratories for Materials Testing and Research* (*EMPA*) *Report No.* 220, 240p. Dynamic behaviour of highway bridge under the passage of heavy vehicles.
6. C. O'CONNOR and T. H. T. CHAN 1988 *Structural Engineering American Society of Civil Engineers*, **114**, 1703–1723. Dynamic wheel loads from bridge strains.
7. T. H. T. CHAN, S. S. LAW, T. H. YUNG and X. R. YUAN 1999 *Journal of Sound and Vibration*, **219**, 503–524. An interpretive method for moving force identification.
8. S. S. LAW, T. H. T. CHAN and Q. H. ZENG 1997 *Journal of Sound and Vibration*, **201**, 1–22. Moving force identification—time domain method.
9. J. S. BENDAT and A. G. PIERSOL 1993 *Engineering Applications of Correlation and Spectral Analysis*. New York: Wiley.
10. S. S. LAW, T. H. T. CHAN and Q. H. ZENG 1999 *Journal of Dynamic Systems, Measurement and Control American Society of Mechanical Engineers*, **121**, 394–401. Moving Force Identification—A frequency–time domains approach.
11. MATLAB Reference Guide. 1992. The MATH Works, Inc.
12. P. PAULTRE, O. CHAALLAL and J. PROULX 1992 *Canadian Journal of Civil Engineering*, **19**, 260–278. Bridge dynamics and dynamic amplification factors—a review of analytical and experimental findings.
13. T. H. T. CHAN, L. YU, T. H. YUNG and S. S. LAW 2001 *Journal of Sound and Vibration* **247**, 77–95. Moving force identification II: Comparative Studies.
14. T. H. T. CHAN, L. YU and S. S. LAW 2000 *Journal of Sound and Vibration* **235**, 87–104. Comparative Studies on moving force identification from bridge strains in laboratory.

APPENDIX A: NOMENCLATURE

The following symbols are used in this paper:

c	speed of moving force
C	viscous damping parameter
$[C]$	damping matrix
E	Young's modulus of material
f	time-varying force
H	frequency response function
I	second moment of inertia of the beam section
L	span length
m	bending moment
M	modal mass
$\{M\}$	nodal bending moment
$p_n(t)$	modal force
$\{P\}$	wheel loads
q	modal amplitude
t	time
v	deflection
x	location along x-axis
$\hat{x}_k$	distance between kth and the first axles
$\{Y\}$	nodal displacement
$\{\dot{Y}\}$	nodal velocity
$\{\ddot{Y}\}$	nodal acceleration
δ	Dirac delta function
Δf	frequency interval

$[\Delta m]$	diagonal mass matrix
Δt	time interval
ε_{ident}	identified value
ε_{true}	true value
ε_{error}	percentage error
ϕ	mode shape function
ρ	mass per unit length
ω	circular natural frequency
ω'	damped circular natural frequency
ξ	damping coefficient
Ψ	Fourier transform of mode shape